

Dynamic QM/MM: A Hybrid Approach to Simulating Gas–Liquid Interactions

Scott Yockel and George C. Schatz

Abstract In this chapter we describe molecular dynamics simulation methods in which the system being studied is divided into a region where quantum mechanics (QM) is used to determine forces for doing Born-Oppenheimer direct dynamics calculations (i.e., doing electronic structure calculations on the fly to determine energies and forces) and another region where empirical potentials that are commonly used in molecular mechanics (MM) calculations are used to determine forces. The two regions are linked through an embedding process that may or may not involve the possibility that atoms can be passed back and forth between regions at each time step. The idea with this dynamic QM/MM methodology is that one uses QM calculations to define the potential surface in portions of the system where reaction occurs, and MM to determine forces in what is typically a much larger region where no reaction occurs. This approach thereby enables the description of chemical reactions in the QM region, which is a technology that can be used in many different applications. We illustrate its use by describing work that we have done with gas–liquid reactions in which a reactive atom (such as an oxygen or fluorine atom) reacts with the surface of a liquid and the products can either remain in the liquid or emerge into the gas phase. Applications to hydrocarbon and ionic liquids are described, including the characterization of reaction mechanisms at hyperthermal energies, and the determination of product branching and product energy distributions.

Keywords Gas-liquid scattering · Hybrid QM/MM molecular dynamics · Interfacial chemistry · Room temperature ionic liquids · Squalane

S. Yockel
University of North Texas, 1155 Union Circle #305398, Denton, TX 76203-5017, USA
G.C. Schatz (✉)
Northwestern University, 2145 Sheridan Rd, Evanston, IL 60208-3113, USA
e-mail: schatz@chem.northwestern.edu

Contents

1	Introduction	44
2	Description of the Method	46
2.1	Basic QM/MM	46
2.2	Dynamic Partitioning via the “Seed Atom” Method	47
2.3	Issues with Dynamic Partitioning	49
3	Simulating Gas–Liquid Interactions	51
3.1	Building a Model Liquid Surface	51
3.2	Gas–Liquid Scattering Model	51
4	Application of Dynamic QM/MM to Gas–Liquid Scattering	53
4.1	Squalane	53
4.2	[emim][NO ₃]	58
5	Summary	63
	References	65

1 Introduction

There are many cases in simulating chemical processes in which the necessary system size to provide a realistic model is quite large (e.g., enzyme reactions, surface phenomena, condensed phase, ...). While the structure and electrostatic interactions in these systems can be well studied with typical molecular mechanics (MM) force fields using molecular dynamics (MD), no chemical reactions (bond making/breaking events) are allowed to take place. On the other hand, it is well established that standard quantum mechanical (QM) methods can compute bond making/breaking with great accuracy; however, the efficiency of these codes limits their practical use to only ~100 atoms on typical computational resources. Even if the computing power was available to handle a larger (~1,000 atoms) QM computation, then it is unlikely that a simulation could be performed for long enough (~10–100 ps) to represent appreciable chemical change in the molecular system. Therefore, dividing up a large-scale system into reactive (bond making/breaking) and nonreactive (electrostatic, steric, interacting vdW, ...) regions is essential.

Research combining QM and MM has an extensive history going back to the early 1970s, and there are numerous review articles [1–12], mostly concerned with enzymatic reactions. A key component of many of these studies concerns the technique used to describe covalent bonds that cross between the QM and MM regions. A common procedure is to add an atom in the QM region where the covalent bond is cut so as to avoid the creation of dangling bonds. This link-atom approach [13] is relatively easy to implement, but there are many variations on what the properties of the link-atom should be [14]. Typically it is taken to be a hydrogen atom, which means that standard electronic structure packages can be used without modification; however in some cases this is not appropriate, or modified hydrogen atom properties should be used. There are also questions about how the QM calculations should be embedded into the overall system. Popular schemes are based on the Morokuma ONIOM scheme or related schemes [15–17], but there

are issues concerning the partitioning of charges between QM or MM regions that keep being refined.

One major difference in the charges in the QM and MM regions is that the MM charges typically do not change during the simulation as they are predefined in the potential force field. The development of QM/MM methods in which the charges from one region dynamically affect those in the other, as would be the case in a true system, is an active aspect of research [18–20]. This approach is referred to as electrical embedding, as opposed to the simple mechanical embedding where the charges are fixed. Evidently, mechanical embedding should be used when charge transfer or long range polarization effects are minimal for the chemical system being studied.

Only a small fraction of the QM/MM studies have explicitly considered molecular dynamics calculations involving both QM and MM regions, as the computational time associated with a QM molecular dynamics calculation is quite demanding. Some examples where this has been done are covered in [21–26]. Recently, our group has developed a simulation model to specifically study reactions at the gas–liquid interface that merges classical MM for the entire system with a QM treatment of the atoms in the reaction region(s) at each time step to form a hybrid QM/MM–MD approach. This new computational approach extends the direct dynamics models our group has used to study gas phase collision chemistry previously [27], and now includes MM calculations for the liquid that is not involved in reactive events. Our primary target liquids have been squalane (for which there are many experiments) and ionic liquids (an unconventional fuel of current interest), and in most cases we have been interested in studying the collision of reactive atoms such as atomic oxygen (O) and fluorine (F) with the liquid surfaces in order to simulate gas–surface molecular beam experiments. In addition, since most of these experiments refer to reactive atoms that have several eV of energy (hyperthermal energies), our applications have been concerned with highly nonthermal processes in which reaction mechanisms that do not normally contribute to thermal kinetics are described.

Projects concerning the O + squalane [28] and F + squalane [29] reaction dynamics have been completed, and they provide detailed information about the spatial distribution of reactive sites and the correlation of the reaction mechanism with the angular and translational distribution of the scattered products. These results have been used to give a detailed mechanistic understanding of beam–liquid surface experiments in the Minton lab [30, 31]. In some cases we were able to identify products not initially considered in the experimental studies, providing stimulus for subsequent molecular beam measurements where they were seen [32]. Our F + squalane studies [29] have been used to interpret experiments done by Nesbitt and coworkers at thermal collision energies [33–35], showing that there is a component of the HF product vibrational and rotational distributions which involves escape of HF from the surface with little relaxation. In more recent work we have considered the collisions of atomic oxygen (and also hyperthermal argon) with the surfaces of ionic liquids [36, 37], providing detailed information about a class of chemical reactions that has not been considered previously, and enabling the interpretation of experiments by Minton, McKendrick, and collaborators.

Our motivation for doing these studies is that the structure and dynamics of chemical interfaces at phase boundaries (e.g., gas–liquid interface) is of significant importance to chemistry and only recently has the capability been established to describe these processes (both with modeling and with experiments) at an atomistic level. Newly developed experimental methods provide the capability to study the reactivity of a liquid surface with beam–surface scattering, which provides detailed mechanistic information, but it is often difficult to interpret these experiments without theoretical modeling. Among the experiments being developed is work by Nesbitt et al. [33–35] who have resolved quantum-state reaction dynamics via direct absorption detection of the rovibrational states of the nascent gaseous products coming from the surface using high resolution infrared spectroscopy. Related technology has been developed by Nathanson [38, 39] and McKendrick [40, 41], who have used laser-induced fluorescence methods to detect the nascent products in gas–liquid surface reaction dynamics studies. In addition, Minton and coworkers [31, 32] have performed molecular beam experiments involving hyperthermal oxygen scattering from liquid surfaces, in which a mass spectrometer is used to determine the angular and translational energy distributions of the nascent gaseous products. These experiments, as well as others, require theoretical modeling that includes the flexibility to compute the dynamics of the reactive events (and sometimes several sequential reactive events), while at the same time the simulation needs to include a considerable portion of the liquid (thousands of atoms) so that energy transfer, diffusion, and electrostatic interactions can be described. Also, the hydrocarbon and ionic liquids are often nanostructured, which means that a simulation region of sufficient size is needed in order to capture all of the dynamical complexity that can occur.

2 Description of the Method

2.1 *Basic QM/MM*

Since most large-scale chemical processes can generally be partitioned into reactive and nonreactive regions, dividing up the system to be treated with different levels of sophistication in the theoretical model is logical. As stated above, the atoms in the reactive parts of the model are treated by direct dynamics QM (electronic structure) computations, while the remaining nonreactive part is treated with an empirical MM potential. Our dynamic QM/MM code utilizes various subroutines from TINKER 4.2 [42] to compute the MM part of the simulation (forces and potential of the MM atoms). For the QM part of the code, subroutines from the MSINDO 2.1 electronic structure code were used [43], which includes the MSINDO (modified symmetrically orthogonalized intermediate neglect of differential overlap) semi-empirical Hamiltonian to compute the energy [44, 45]. In general, semiempirical methods are a middle ground between a fully ab initio QM calculation and fully

empirical MM potentials and are suitable for efficiently computing the electronic structures of hundreds of atoms in a reasonable time (seconds) to be used in dynamics. In comparison to other standard semiempirical methods, MSINDO provides reaction energies and barriers for gas-phase reactions of atoms with small hydrocarbons that are nearer to experimental values than AM1 and PM3 [27]. Therefore, it has been the QM method of choice for our studies on $\text{O}(^3\text{P})$ and $\text{F}(^2\text{P})$ with squalane. Additionally, we have used MSINDO when studying $\text{O}(^3\text{P}) + [\text{emim}][\text{NO}_3]$, a room temperature ionic liquid.

Many of the features of the nondynamic QM/MM model, which has been widely used as a multilevel computation, exist in our dynamic QM/MM algorithm. When bonds straddle the QM/MM boundary, the link atom method is employed to truncate the QM region without leaving dangling bonds. For example, if a C–C bond spans this boundary, then the C(MM) atom is replaced with an H(QM) atom at 0.9 Å (the equilibrium C–H bond length) from the C(QM) during the QM part of the computation. During a full QM/MM computation, three separate calculations are performed, as prescribed by the ONIOM mechanical embedding approach. In the following notation, the atomic system is denoted in parenthesis. First the full atomic system is computed with MM, $[E_{\text{MM}}(\text{QM} + \text{MM})]$. Then the QM atomic system is computed with MM $[E_{\text{MM}}(\text{QM})]$, and the QM system with QM $[E_{\text{QM}}(\text{QM})]$. Therefore, the energies, potentials, forces and other properties are computed as follows: $E_{\text{QM/MM}} = E_{\text{MM}}(\text{QM} + \text{MM}) - E_{\text{MM}}(\text{QM}) + E_{\text{QM}}(\text{QM})$.

Subtracting $E_{\text{MM}}(\text{QM})$ from $E_{\text{MM}}(\text{QM} + \text{MM})$ is an approximation that describes electrostatic interactions between charges in the QM and MM regions at the MM level. The importance of this depends on the system being studied and the choice of partitioning at the QM/MM boundary, but it is consistent with the assumptions in the mechanical embedding model. In the case of our studies with squalane, the system is a neutral nonpolar liquid and charge transfer between interacting atoms from inside to outside the reactive region is thought to be negligible; therefore a simple mechanical embedding approach was chosen. Additionally, we rely on this assumption, as discussed later, when we allow the QM region to change over time.

One of the most common numerical methods used in molecular dynamics to solve Newton's equations of motions is the Velocity Verlet integrator. This is typically implemented as a second order method, and we find that it can become numerically unstable during the course of hyperthermal collision events, where the atom velocities are often far from equilibrium. As an alternative, we have implemented a fifth/sixth order predictor–corrector scheme for our calculations. Specifically, the driver we chose utilizes the Adams–Bashforth predictor method together with the Adams–Moulton corrector method for approximating the solution to the equations of motion.

2.2 Dynamic Partitioning via the “Seed Atom” Method

In some simulations, like that of large biological systems that involve reactive sites and proton transfer, the choice of a reactive region does not change while the

reaction occurs and the QM/MM scheme is easily implemented. However, there are many chemical systems in which a priori knowledge about where the reactive region will be during the course of the simulation is not predictable by chemical intuition. Within our group we have had success employing a simplistic approach to a QM/MM–MD algorithm that is applicable to chemical systems where a priori knowledge is largely unavailable as to which atoms should be considered as part of the reactive region [28, 29]. This is specifically the case when gaseous atoms collide with an amorphous surface that can readily diffuse over time. For example, in our studies with squalane we even found that the incident atom was not always confined within a ~ 20 Å (radius) \times 20 Å (height) cylindrical box that contains over 2,000 atoms comprising the liquid. This is not the situation that is observed with crystal-line solids or self-assembled monolayers. When modeling those surfaces, one can predefine atoms into a QM region because the incident atoms would rarely interact with more than the first or second monolayer.

In order to circumvent the limitation of predefining which atoms are to be treated with QM, we allow atoms to be redefined dynamically as “in” or “out” of the reactive region depending on their location relative to radical species that are capable of undergoing a reaction. Specifically, the reactive regions are centered around “seed atoms”, which are defined as all of the open-shell/radical atoms. In the case of our studies involving atomic radicals reacting with squalane, the seed atoms were defined as the initial gaseous incident atom plus, over the course of the simulation, any atom that loses one of its originally bonded atoms. For example (see Fig. 1), if the $F(^2P)$ atom abstracts a H from squalane, then the carbon radical

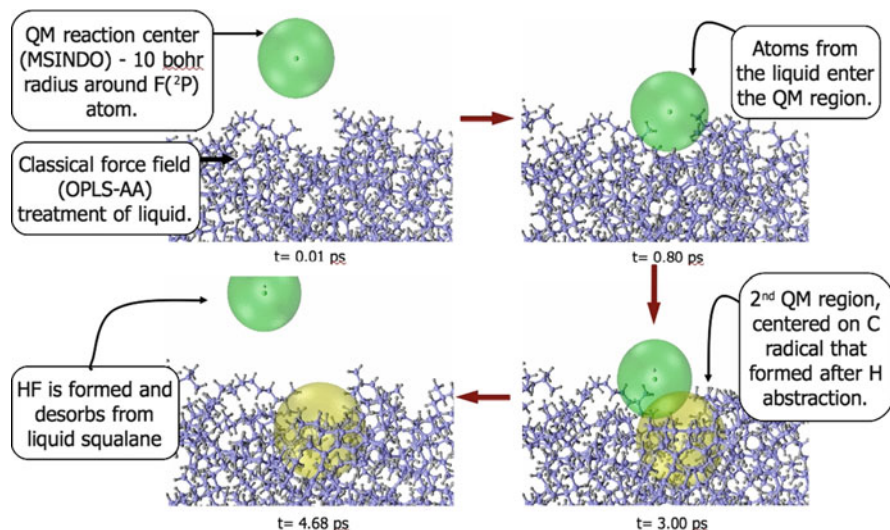


Fig. 1 Pictorial representation of the dynamic partitioning using the “seed atom” method for the $F(^2P)$ + squalane reaction

site also becomes a seed atom, since this radical site is considered to be a reactive atom. The radius of the QM region around a seed atom (or the distance from the seed atom to atoms treated as MM) was defined as the distance where the forces between the atoms are less than 1×10^{-7} hartree/bohr, at which point the differences between MM and QM forces are thought to be negligible. This was empirically determined to be 10.0, 10.0, 12.0, 12.5 bohr for F, O, H, and C, respectively, when interacting with methane. We also found it convenient to do an assessment on which atoms should or should not be in the reactive region only every ten time steps, since this involves a distance search and, for 10-a.u. time steps, the atoms have not moved very far. Throughout much of the simulation it is common to have between 75 and 150 atoms within the reactive region(s). Given the effort associated with QM calculations at each time step, the use of a computationally efficient semiempirical QM method such as MSINDO is clearly desirable.

2.3 *Issues with Dynamic Partitioning*

It must be noted that the instantaneous switching of an atom in and out of the reactive region has raised concern in the past [21]. This is because from one time step to the next there will inevitably be an abrupt change in the forces on that atom. In dynamics studies this discontinuity can influence the integration with respect to time and conceivably lead to nonphysical behavior. To circumvent this we use a more robust integration method (a sixth order predictor–corrector algorithm) that is not available in TINKER. This integration technique should help dampen out any fluctuations in the force/position changes that would lead to discontinuities when atoms are switched back and forth between the MM and QM regions.

Recently other groups have designed algorithms that include dynamically moving QM regions to model explicit solvent interactions. Morokuma et al. have extended their multilevel ONIOM technique to include the exchange of solvent (ONIOM-XS) molecules dynamically throughout the simulation [23]. They implemented a fifth order polynomial switching function to accommodate the instantaneous change in forces and potentials on atoms changing from one level to the next in the ONIOM regime. This technique extends the “Hot Spot” method that Rode et al. originally used [46] by not only smoothing out the differences in forces of atoms that are in a defined “buffer” region between the various levels, but also smoothing out the forces for all atoms in the QM region when any atom crosses in or out of the buffer region. In addition, the ONIOM-XS method uses the same switching function algorithm to smooth the potential energy for the atoms in the QM and buffer regions. However, knowing how large the buffer region needs to be for each chemical system is uncertain. Furthermore, it has been demonstrated that when multiple molecular groups are in the buffer region the ONIOM-XS method is no longer able to remove all discontinuities in the potential [23].

Truhlar and coworkers have developed an elaborate algorithm for smoothing the forces and the potential of the atoms switching regions in order to conserve both energy and momentum [21]. Their adaptive partitioning (AP) method is able to fix the conservation problem in a long time regime (400–1,000 ps), and they suggest using their permuted AP method when dealing with equilibrium conditions, a situation when energy or momentum drift could noticeably influence the physical or chemical behavior of the system. The permuted AP method does however include a number of multilevel computations at each time step (as opposed to just one) in order to assess how the potential smoothing functions are applied. This increases the number of computation by 2^N for each N groups in the buffer zone. By our estimates, in the squalane system ~ 4.4 carbon atoms would be in the buffer zone on average, thus increasing the QM calculations by >21 times and making the AP method unattractive when thousands of trajectories are needed.

In both of the algorithms just described, only small solvent molecules (e.g., H_2O , NH_3 , ...) are present in the simulations, and these molecules never straddle a boundary. The use of switching functions when an atom or small molecule is in a buffer region is convenient when the solvent molecule does not span from inside the QM region, through the buffer, and into the MM region. In this situation, the buffer region atoms are being given some MM character while still being bonded to atoms in the QM region, which could lead to extraneous forces on all the QM atoms in that molecule. This makes the inclusion of such algorithms to our current model nontrivial. Additionally, it must be noted that in our simulations we are not concerned with equilibrium conditions since the incident atom collides at the surface with 1–5 eV of translational energy. Furthermore, our simulation times are <10 ps, at which appreciable energy or momentum drift should be very minimal.

Though we had success with dynamic partitioning with squalane, when we began to study gas–liquid collision chemistry of room temperature ionic liquids, dynamic partitioning as we had done in the past became problematic. This is because the liquid, 1-ethyl-3-methyl-imidazolium nitrate or [emim][NO_3], is composed of cations and anions, and each of these cannot meaningfully be divided into parts in the QM and MM region. This would require some sort of charge partitioning algorithm, likely requiring charges to switch back and forth between regions as a function of time, resulting in extraneous forces. Because the liquid is ionic, it has slower diffusion and much higher density than the hydrocarbon liquids, preventing the surface from changing much over time. After testing numerous trajectory paths, we found that it was rare that the incident atom with an $E_T \leq 5.0$ eV had a direct interaction with more than the first two ion pair layers. Therefore we decided to fix the QM region to include five ion pairs (115 atoms) at or near the surface and the incident $\text{O}(^3\text{P})$ atom. In comparison to squalane, where there were often several well separated radical species, $\text{O}(^3\text{P}) + [\text{emim}][\text{NO}_3]$ can be treated with a more localized QM description.

3 Simulating Gas–Liquid Interactions

3.1 *Building a Model Liquid Surface*

Prior to the scattering of a gaseous atom off of a liquid surface, a properly equilibrated surface must be created. Initially, we have created a bulk model of the desired liquid with the TINKER program by using the OPLS all-atom force field [47] and the isobaric–isothermal (NPT) ensemble for ~ 1.0 ns at 400 K with periodic boundary conditions applied. This ensures that the fluctuations in bulk density have reached a minimum. Afterward, the final structure of this simulation is used as the initial structure for an additional NPT simulation which is cooled to 298 K (or some arbitrary experimental temperature) for ~ 0.5 ns at which the average bulk density is measured in comparison with physical property values. In our work with squalane ($\text{C}_{30}\text{H}_{62}$) the density was found to be 0.769 g/cm^3 , compared to the observed value of 0.815 g/cm^3 . To create a liquid surface, at this point the periodic boundaries in one direction are extended by a factor of three so that two empty vacuum regions are present on top and bottom of a slab of the equilibrated bulk liquid. This system is then run for ~ 1.0 ns with the NVT ensemble to allow for surface relaxation of the bulk liquid. After the surface density has equilibrated, random snapshots of the surface are used as the starting surface for the reactive scattering simulations. It is these surfaces that are used to compute the average surface density profiles, which enables us to analyze the types, locations, and orientations of different molecules (or parts of the molecule, like functional groups) within the liquid.

In our previous work, we were able to show that, even though the bulk squalane contains twice as many secondary carbons as primary or tertiary, at the surface the majority of the carbons are primary and stick up out of the surface (see Fig. 1). It is important to understand what types of atoms are on the surface as their reactivity is what drives the surface chemistry. Additionally, with our [emim][NO_3] surface we found that the anion is more abundant at the surface than the cation and that the ethyl-chains that lie on the surface tend to stick up towards the vacuum [37]. However, we found that there exists a slightly different surface topology for [emim][NTf_2], which includes a larger anion that keeps the ethyl chain from protruding out of the surface [36]. In contrast, the surface of [C_{12}mim][NTf_2] has long hydrocarbon chains sticking up into the vacuum, causing a noticeable difference in the reaction profile that occurs upon gaseous atom collision.

3.2 *Gas–Liquid Scattering Model*

In order to simulate gaseous atoms scattering from a liquid surface that represents a realistic sampling of the various chemical and surface features, various input conditions should be considered to enable a connection to the experimental conditions. The following conditions are what we have chosen for our models. After an

equilibrated surface has been generated, multiple snapshots that are well separated in time are used as the input for the scattering surface. Each of these snapshots represents a unique surface, and several such surfaces are sampled in the trajectory calculations. Because of the nature of the QM/MM calculation, periodic boundaries are not used, and therefore, to keep the surface density consistent over the time of the simulation, we fix the coordinates of atoms in the outer walls and base of the liquid as shown in Fig. 2 for O + [emim][NO₃]. The incident atom is directed to collide with the surface at locations that are chosen from a series of grid points spaced ~ 2.5 Å apart to ensure sampling of the various functional groups or atom types that are present at the surface. In order to understand the angular dependence of the scattering and not bias the incident atom to a particular angle of incidence, several azimuthal angles are sampled and results are considered from different incident polar angles (θ_i) relative to the surface normal. Figure 3 provides a schematic representation of this basic setup, which was utilized in our various gas-liquid scatter experiments. In the case of our O/Ar + [emim][NO₃] studies, ten unique surfaces, nine points on the surface grid, four azimuthal angles (0° , 90° , 180° , 270°), and four incident polar angles (0° , 30° , 45° , 60°) are considered for

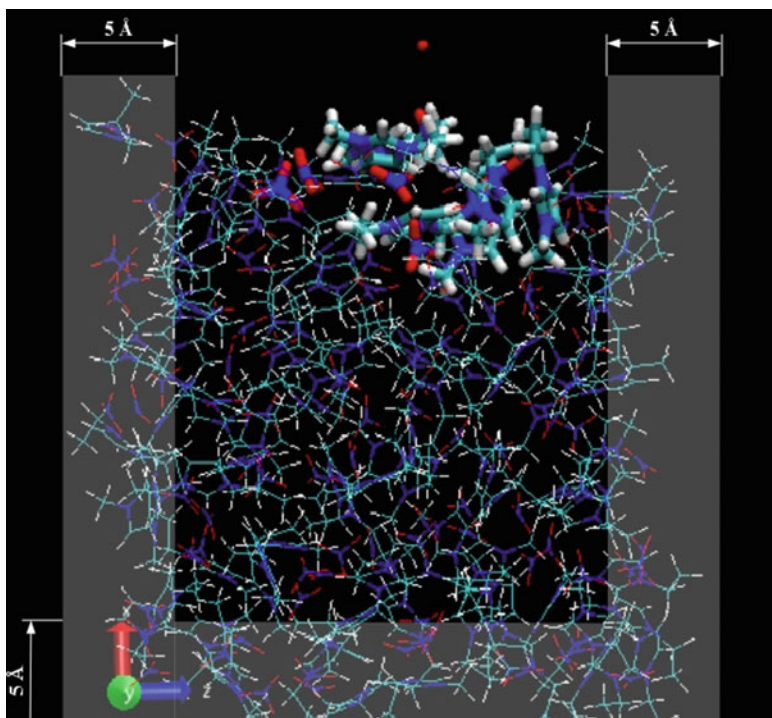
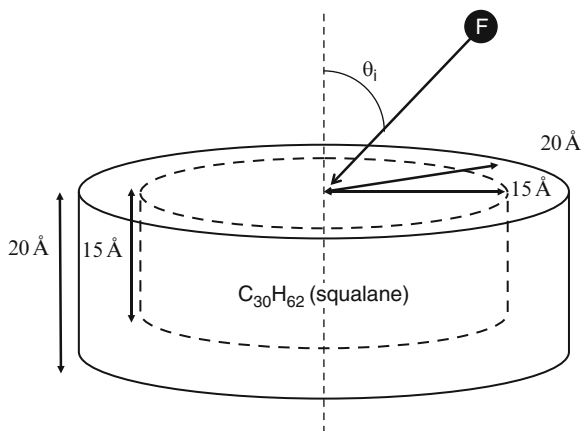


Fig. 2 Side view depiction of the $32.3 \times 34.5 \times 31.6$ Å³ QM/MM simulation box of O + [emim][NO₃]. The *sticks* represent the 2,093 atoms computed with MM and the *tubes* are the 116 atoms computed with QM. Atoms within the 5 Å thick shaded regions on the sides and bottom are the MM atoms kept fixed during the simulations to keep the liquid density from changing over time

Fig. 3 Schematic picture of the simulation region. The *outer region* is composed of fixed coordinate atoms while atoms in the *inner region* are allowed to move freely.

Arrows indicate the trajectory of the incident fluorine atom with angle of incidence θ_i



a total of 1,170 trajectories. For this chemical system there exist ~40–60% scattered nascent products, which provide a large enough sample set to compute statistical averages.

4 Application of Dynamic QM/MM to Gas–Liquid Scattering

4.1 Squalane

Squalane ($C_{30}H_{62}$) is a branched hydrocarbon with very low vapor pressure. It is a popular liquid for molecular beam experiments as the chance that atoms in the beam will collide with molecules evaporating from the liquid is sufficiently low; thus the beam atoms can move ballistically, and reactions will only occur at the interface. Experiments from Nesbitt et al. [34, 35] and Minton et al. [31, 32] have demonstrated that, with incident $F(^2P)$ or $O(^3P)$ atoms, there exist two distinct reactive processes with squalane. When the incident atom and nascent products have very few collision events and spend very little time (on the order of ps) in the liquid, the products leave the liquid with velocities and internal states that are largely reflective of the primary reactive event. For hyperthermal initial conditions, this mechanism is referred to as the hyperthermal desorption/scattering (HDS) component. On the other hand, the incident atom and nascent products may have many collisions, spending significant time in the liquid (ns– μ s). In this case, the products leave the surface with comparable energy to the surface temperature, and the mechanism is referred to as the trapped desorption (TD) component. Due to current computing resource limitations, our current dynamic QM/MM can only simulate <10 ps of these reactions. Thus, any TD products coming from the liquid are missed; these products are still trapped in the liquid at the termination of the simulation.

We have completed two complementary gas/surface collision studies with squalane, using incident $O(^3P)$ with 5 and 1 eV and $F(^2P)$ with 1 and 0.5 eV initial translational energy [28, 29]. To understand the viability of using MSINDO for the QM method, we computed the reaction enthalpies and barriers for the H abstraction and elimination reactions of O/F with methane and ethane, and compared the results to those from the advanced ab initio method CCSD(T). These comparisons show that for the reaction barriers, which are important for the bond making/breaking events in our simulations, the MSINDO computations are comparable (~ 0.15 eV) to the CCSD(T) results. For the methane reaction, the H abstraction reaction ($O + CH_4 \rightarrow CH_3 + OH$) has an $\Delta E_{rxn} = -0.342$ eV whereas with F the reaction is more exothermic (as expected) with an $\Delta E_{rxn} = -1.418$ eV, based on MSINDO. Also, the reaction barriers are completely distinctive for these two reactions, with the barrier for $O + CH_4$ being 0.564 eV and that for $F + CH_4$ only 0.167 eV. The H elimination reaction ($O + CH_4 \rightarrow CH_3O + H$) has a quite different thermochemistry with a $\Delta E_{rxn} = 0.081$ eV while that for $F + CH_4$ is $\Delta E_{rxn} = -0.015$ eV; the reaction barriers are 1.869 and 1.769 eV, respectively. Generally, the MSINDO computed thermochemistry with ethane has slightly lower reaction barriers as compared to methane for both the H abstraction and elimination channels.

Considering the differences in thermochemistry between F and O reactions with methane and ethane, it is not surprising that in our F + squalane studies, with incident energies of 1.0 and 0.5 eV, no H elimination reactions are found; in contrast, in O + squalane with the incident energy of 5 eV the probability of an H elimination reaction is as high as 0.14. Additionally, in the O collision studies double H abstraction and C–C bond cleavage occur with probabilities as high as 0.22 and 0.06, respectively. Another interesting difference in these two reactions is in the probability that the product does not desorb from the surface by the end of the simulation time (~ 10 ps). Upon H absorption, HF has a desorption probability of 0.90–0.95 (dependent on incidence angle), while OH has a bit lower probability of 0.71–0.83. This may be in part due to the average depth of penetration of the incident atom before the reaction occurs, whereas the O average depth for H abstraction is ~ 0.5 Å deeper than for F. Also, HF is formed with a higher probability than OH, with reaction probabilities of 0.78 and 0.41, respectively, which is understandable given that the MSINDO reaction barriers for H abstraction (of methane or ethane) are ~ 3 – 4 times higher for O than F. However, the copious formation of HF does not necessarily translate into the efficient transfer of the incident energy into the product’s vibrational, rotational, and translational modes.

To examine these results in more detail, we now look at how the vibrational states of the HDS component for the H abstraction product are affected by the choice of F or O as the reactant. We compute these vibrational states based on the classical histogram method [48], wherein the vibrational quantum numbers (calculated from the vibrational action [49]) is rounded to the nearest integer to determine vibrational state populations. A similar method is used to define rotational quantum number starting from the classical rotational angular momentum.

The dynamic QM/MM calculations show that the nascent gaseous product HF leaves the surface with nearly all its vibrational distribution in either the

$\nu = 1$ or 2 state, and is split fairly equally between them. This is similar to what is seen for gas phase reactions of atomic fluorine with hydrocarbons, indicating that there is only modest vibrational relaxation as the HF exits the liquid. For the OH product, most of the vibrational distribution is in $\nu = 0$, with only a fraction (0.13) being in the $\nu = 1$ state. This reflects the smaller energy release in this reaction, together with inefficient conversion of reagent kinetic energy into product vibrational energy (as is also known from gas phase analogs). When the incident energy of O is lowered from 5 to 1 eV there is even less population of OH in the $\nu = 1$ state, with a probability of only 0.05. On the other hand, when changing the incident energy of F from 1.0 to 0.5 eV, there is a decrease in the $\nu = 0$ population and an increase in the $\nu = 2$ population. The vibrational distribution of HF with the lower incident energy of 0.5 eV is more closely aligned with the experimental results from Nesbitt et al. where the incident energy is ~ 0.08 eV. This indicates that the population of the product vibrational modes is not governed by the incident energy of the colliding gaseous atom, but is mostly due to the release of energy in the bond breaking event.

Some of the energy released during the reaction is also transferred into the rotational states of the nascent products. Figure 4 presents the distribution of rotational states of HF for the major vibrational states. For the $\nu = 1$ state of HF, the distribution of rotational states is largely unchanged by the incident energy, while for $\nu = 2$, there are slightly hotter rotational states from the 0.5 eV initial energy. A more drastic change in rotational distribution can be seen when changing

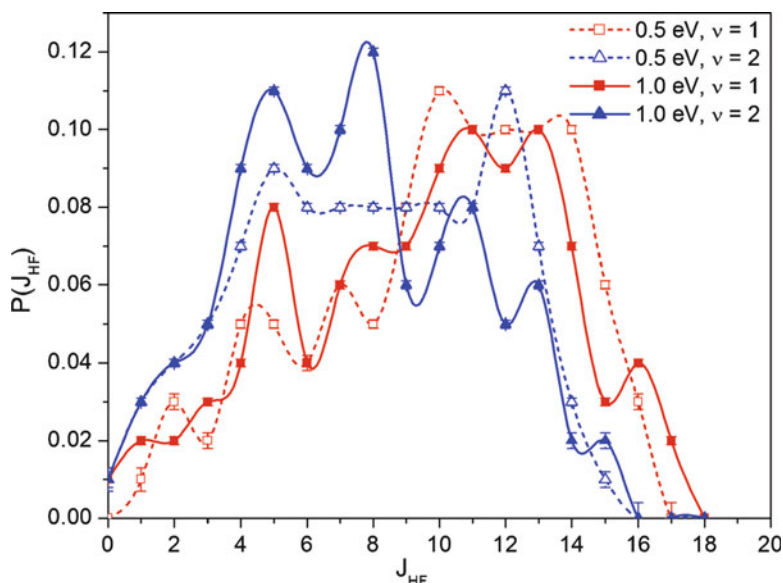


Fig. 4 Distribution of rotational states for the $\nu = 1$ (red) and $\nu = 2$ (blue) vibrational states of HF, as obtained from F + squalane simulations. Solid lines are for 1.0 eV and dashed lines are for 0.5 eV input translational energy

the incident energy of O from 5 to 1 eV. With 5.0 eV incident energy, the OH rotational distribution peaks around $J = 5$ –6 and has a bit of a Boltzmann-like distribution. On the other hand, with 1 eV incident energy the OH rotational distribution is hotter and peaks around $J = 10$ –12. This is further evidence that the transfer of energy into the product states is not governed by the incident energy.

Comparing translational energy distributions provides another contrast of the results from F vs O. Here we compare the H abstraction products (OH and HF) as well as the inelastic scattered atoms (O and F). For both inelastically scattered products there is a similar variation of final translation energy distribution with respect to angle of incidence. At 60° angle of incidence there is a broad distribution of translational energies, covering the range from almost zero energy to an energy equal to the incident energy (i.e., 1.0 eV for F and 5.0 eV for O) as shown in Figs. 5 and 6. By contrast, at 30° angle of incidence, most of the input translational energy is transferred into the liquid.

There is a notable difference in the final translation energy of the H abstraction products, OH and HF. The OH final translational energies are very similar to the O energies and still have a distinctive variation with respect to the incidence angle. In contrast, the HF product final translational energies are largely independent of

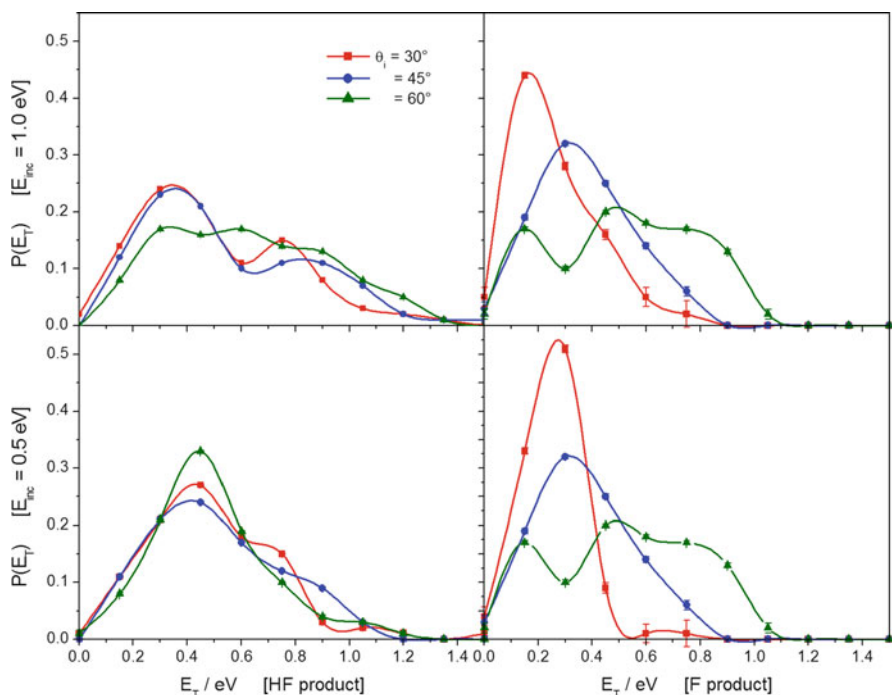


Fig. 5 Distribution of product translational energies in eV of HF (*left*) and scattered F (*right*) from incident translational energies 1.0 eV (*top*) and 0.5 eV (*bottom*) and for each angle of incidence 30° , 45° , and 60°

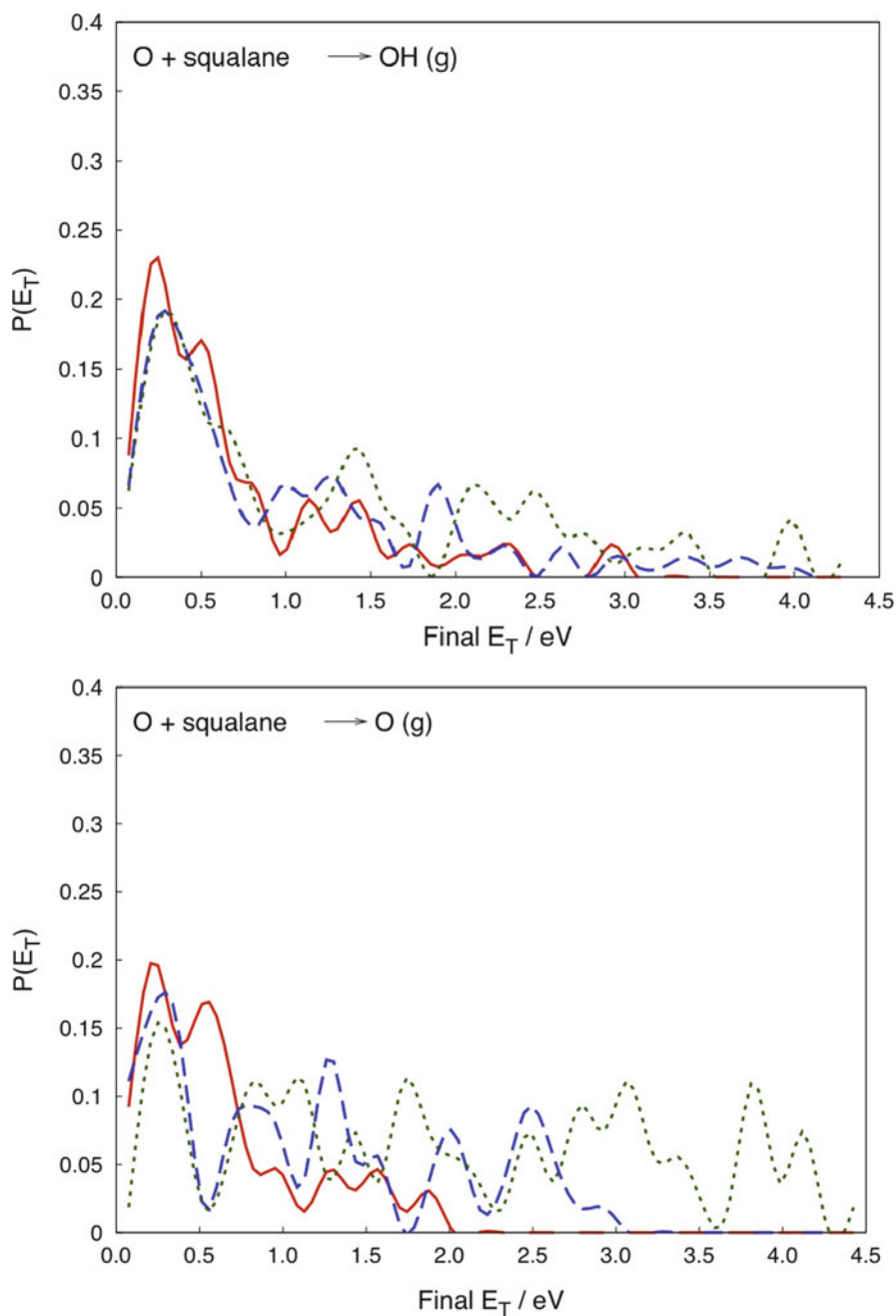


Fig. 6 Distribution of product translational energies in eV for OH (*top*) and scattered O (*bottom*) for O + squalane collisions with an incident translational energy of 5 eV and for each angle of incidence 30° (solid red), 45° (dashed blue), and 60° (dotted green)

incidence angle in comparison to the scattered F energies. Also, there is very little difference in the final translational energy of the HF product with regard to input translational energy. Furthermore, for the 0.5 eV incident energy it is even common that the HF product has more final translational energy than F had initially. This brings clarity to the notion that the molecular energy transferred to the product states is mainly from the chemical reaction that takes place and not from the collision energy.

4.2 [emim][NO₃]

We have also applied our dynamic QM/MM model to study the surface reactivity of room temperature ionic liquids (RTIL). These RTIL are quite unique liquids in that they are comprised solely of cation and anion pairs that can be interchanged with other types of cations or anions; therefore, their physical and chemical properties are a bit tunable. Generally these liquids are nonvolatile and nonflammable, chemically and thermally stable, and possess high ionic conductivity. Our interest in RTIL is in their use as environmentally conscious hypergolic bipropellants. Although these liquids are becoming more readily utilized as solvents, little is known about the surface reactivity of these liquids. Since we have had some success in analyzing the reactivity of squalane via gaseous atom/surface scattering, we extended our work to include a simple RTIL, 1-ethyl-3-methyl-imidazolium nitrate, referred to as [emim][NO₃]. This liquid can be viewed as three distinctive components – the NO₃ anion, the imidazolium ring cation, and the nonpolar hydrocarbon tail (ethyl-chain) – all with their own unique local chemistry.

The [emim][NO₃] RTIL was chosen because an OPLS-AA force field had already been developed for it [50], and it limits the chemical interactions to only C, H, O, and N, atoms for which we have confidence in using MSINDO to predict reasonably accurate thermochemistry of nitrogen-containing ring systems [51, 52]. In order to grasp the difference in the reactivity of the different surface components with each other. As opposed to the incident atom, we chose to compare the nonreactive scattering of Ar with the surface to the chemistry that results in reactive scattering with O(³P), both with an initial 5.0 eV of translational energy.

The gas–liquid scattering setup is very similar to that described with the squalane experiments in the previous section. However, as mentioned in Sect. 2.3, the QM region in these simulations was fixed to a localized region near the surface. Our surface analysis of [emim][NO₃] indicates that the ethyl-C sticks up out of the surface, followed by an even distribution of cations and anions. This means that there are readily accessible H atoms sticking up out of the surface for H abstraction or H elimination reactions to occur before the incident O crosses the surface threshold (the point where the density is equal to half the bulk density). Our study was done in tandem with Minton and coworker’s similar experimental study [36] that used the RTILs [emim][NTf₂] and [C₁₂mim][NTf₂], which they are able to obtain with high purity, unlike [emim][NO₃] at the time of their study.

In both of these liquids the computed surface topology demonstrated that the large anion and the ethyl-chain are equally present at the surface, while the longer C₁₂-chain extends well out of the surface, thus exposing a significant amount of accessible H to the incoming O atoms.

Upon collision with Ar, some translational energy is transferred into the [emim][NO₃] surface causing minor changes in the local chemistry as shown in Table 1. Nearly all of the incident Ar atoms scatter from the surface (a probability of 0.91) with a small fraction trapped at the end of the simulation time of 7.3 ps. The momentum transfer causes on average two to three proton transfers to occur between the imidazolium ring and the anion (see Table 2), thus neutralizing the

Table 1 Probabilities for scattering Ar and O(³P) from an [emim][NO₃] surface, including the distribution of each nascent product

	From Ar	From O(³ P)
Total ^a	0.17 ± 0.01	0.57 ± 0.02
Incident atom ^b	0.91 ± 0.03	0.23 ± 0.01
HNO ₃	0.06 ± 0.01	0.04 ± 0.006
emim ^c	0.10 ± 0.01	0.12 ± 0.01
<i>emim</i> + [NO ₃] ^d	0.01 ± 0.003	0.05 ± 0.006
O	–	0.13 ± 0.01
OH	–	0.04 ± 0.005
O ₂	–	0.02 ± 0.005
HNO ₂	–	0.05 ± 0.007
Me/Et fragment ^e	–	0.02 ± 0.005
IM-chain ^f	–	0.01 ± 0.003
IM-chain fragment ^g	–	0.04 ± 0.006

^aFor Ar this value includes the sum of all non-Ar products; for O, this includes all desorption products

^bIncludes only desorption products containing the incident atom

^cRefers to the neutral species from the cation [emim] after loss of H⁺

^dRefers to any pairs or groups derived from the imidazolium ring (cation or neutral) with the anion

^eMethyl or ethyl fragment from elimination of hydrocarbon from ring

^fThe unfolded imidazolium ring from ring scission – O addition

^gA piece of the unfolded ring from ring fragmentation – O addition

Table 2 Distribution of number of proton transfers and cation/anion pair recombinations

Proton transfer	Incident O	Incident Ar
0	0.12 ± 0.01	0.13 ± 0.01
1	0.29 ± 0.02	0.21 ± 0.01
2	0.35 ± 0.02	0.31 ± 0.02
3	0.20 ± 0.01	0.30 ± 0.02
4	0.04 ± 0.01	0.05 ± 0.01
5	0.00	0.00
[emim] + [NO ₃] → emim-ONO ₂ ^a	0.12 ± 0.01	0.12 ± 0.01

^aAn oxygen from NO₃ attaches to the imidazolium ring

cation/anion pair. Once neutralization occurs, it is inevitable that the neutral species will eventually desorb from the charged liquid. Instead of proton transfer, the surface collision can also supply enough energy to enable the anion to react with the cation. This bond usually occurs between an O in $[\text{NO}_3]$ and one of the C–H carbons on the imidazolium rings. It is likely that these recombinations with the cation and anion are only short lived in the actual system. However, within our simulation time, we found that the probability of these events was 0.12. When the proton transfer event occurs to a molecular species that is located at the surface edge, there is sometimes enough momentum to “push” the neutral species off of the surface, which is listed as “total” in Table 1. The probability for this event to happen to [emim] is 0.10 and for $[\text{NO}_3]$ is 0.06. There is only a very slight probability of 0.01 that more than one molecular species departs the surface together. Overall, for nonreactive scattering of Ar from the surface, little change occurs chemically to the ionic liquid molecules. This adds to knowledge concerning the chemical and thermal stability of RTIL.

The collision of a reactive atom, $\text{O}(^3\text{P})$, with [emim] $[\text{NO}_3]$ causes a multitude of chemical reactions to ensue at the surface. This is in contrast to the scenario that we just presented with the bombardment with Ar, a nonreactive atom, although there are some common features as well. The types of reactions that occur have been grouped into reaction types in Table 3. One of the most common reactions, with a probability of 0.43, is the elimination of NO_3 , which occurs when the incident O collides with $[\text{NO}_3]$ forming NO_2 or HNO_2 and O_2 or occasionally OOH . The second most prevalent reaction type, occurring with a probability of 0.21, is ring scission – O addition; this occurs when O addition causes a bond scission in the imidazolium ring, opening it up into an intact chain. About a quarter of the time there is enough vibrational energy in the chain that it splits apart creating the channel labeled ring fragmentation – O addition. Commonly, in both the ring scission reaction types, an aldehyde is formed. As with the O + squalane reactions, H abstraction also occurs in the O + [emim] $[\text{NO}_3]$ reaction yielding OH with a probability of 0.09. Note that this is much lower than the 0.41 that is found with

Table 3 Reaction probability from $\text{O}(^3\text{P}) + [\text{emim}][\text{NO}_3]$ by reaction type

Distribution of reactions by type	
O scattering	0.13 ± 0.01
O addition to NO_3	0.02 ± 0.004
Elimination of NO_3	0.43 ± 0.02
O addition to HC^{a}	0.01 ± 0.002
Elimination of HC from ring	0.04 ± 0.01
Ring scission – O addition ^b	0.21 ± 0.01
Ring fragmentation – O addition ^c	0.05 ± 0.01
H abstraction	0.09 ± 0.01
NO_3 substitution	0.01 ± 0.003
HC substitution – H elimination	0.02 ± 0.004

^aHC refers to the ethyl or methyl hydrocarbon on the imidazolium ring

^bAfter ring scission the [emim] becomes an intact chain

^cAfter becoming a chain, fragmentation occurs

squalane, which makes sense since the ionic liquid has a smaller fraction of abstractable hydrogens. There is a small chance, 0.13, that the O does not react and bounces back from the [emim][NO₃] surface; inelastic collisions of this nature with O + squalane occur more often, with an overall average probability of 0.23.

In the O + [emim][NO₃] collisions, more than half of the products desorb from the surface during our simulation time, as shown in Table 1. This is in contrast to the Ar collision study where the probability of non-Ar containing products was 0.17. As with the nonreactive study, the O collisions also cause one to three proton transfers (see Table 2). Interestingly, a similar portion of HNO₃, emim, and *emim* + [NO₃] desorb from the [emim][NO₃] surface as compared to the nonreactive study; HNO₂ is an additional product found in the O scatter data. It is likely that the proton transfer event is responsible for these species desorbing from the [emim][NO₃] surface. The H abstraction channel, which occurs predominantly at the ethyl or methyl sites on the imidazolium ring, forms OH and has a desorption probability of 0.04. Nearly half of all the OH created desorbs from the surface by the end of the simulation (7.3 ps). In squalane, around 80% of the OH exits the surface. This is reflective of the differences in the surface density and the amount of diffusion that is possible within these two liquids. It must be noted that no charged species were found to desorb, which is not surprising because they would inevitably be attracted back to either the cations or anions at the surface.

In connection with the experimental observables that Minton et al. have measured for the similar reaction (O + [emim][NTf₂]), we also report the translational energy distribution of the inelastically scattered atoms as well as of the major molecular products. Figure 7 provides a basis for understanding how the [emim][NO₃] liquid is

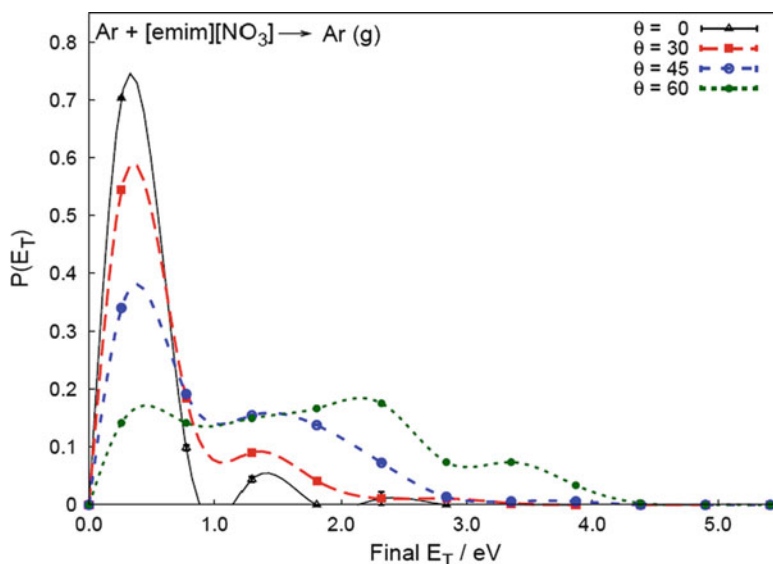


Fig. 7 Distribution of the final translational energy (in eV) of Ar for each angle of incidence ($\theta_i = 0^\circ, 30^\circ, 45^\circ$, and 60°)

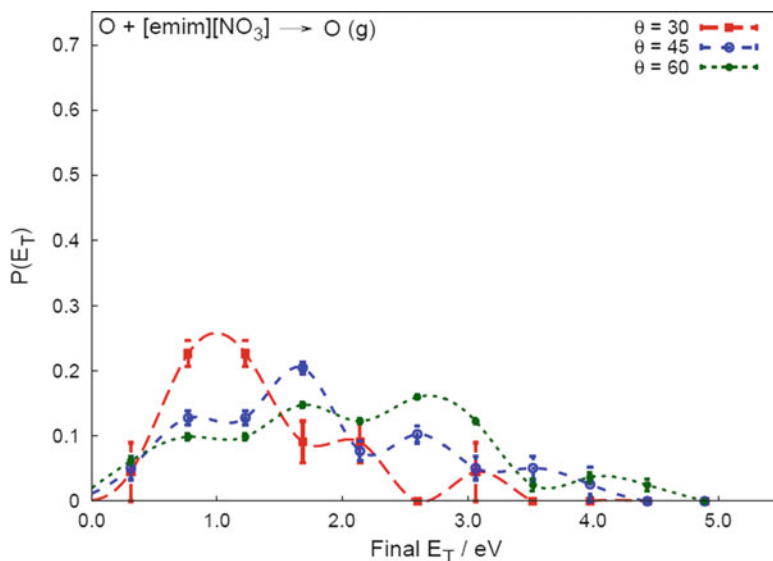


Fig. 8 Distribution of the final translational energy (in eV) of $\text{O}(^3\text{P})$ for each angle of incidence ($\theta_i = 0^\circ, 30^\circ, 45^\circ$, and 60°)

able to absorb energy upon bombardment by a nonreactive atom. Overall there is a broad distribution of final translational energies from the more glancing angle of 60° , and on average about half the 5.0 eV initial energy is transferred to the liquid. For more direct angles of incidence, nearly all the final translational energy is below 1.0 eV, indicating that multiple collisions play an important role. Figure 8 shows the corresponding results for inelastically scattered O atoms. (No 0° data are presented because almost all the incident Os undergo reaction for this angle.) For an incident angle of 60° , there is a very similar distribution of final translational energies for O as was found with Ar. This is likely due to the fact that at this glancing angle there is very little penetration of the surface (0.94 \AA for Ar and -0.68 \AA for O on average), thus minimizing the number of collisions and leaving the incident atom mostly unchanged. For the more direct collisions at 30° and 45° , the scattered O has more translational energy than Ar, as if the larger, heavier Ar atom is a “softer” atom losing more energy to the liquid. The distribution of final translational energy from the OH desorption product is depicted in Fig. 9. There is a slight decrease ($\sim 0.5 \text{ eV}$) in the translational energies of the OH product in comparison to the inelastically scattered O, with similar distributions between the various angles of incidence. Most of the OH products are from H abstraction at the C–H groups on the ethyl and methyl substituents on the imidazolium ring, which are sticking up out of the surface. On average, at 60° incidence angle, both O and OH scatter from [emim][NO_3], as we found with our QM/MM–MD model, with about half the initial translational energy; this coincides with the experimentally determined final translational energy of O and OH scattering from [emim][NTf_2]. Other nascent products, which are not shown

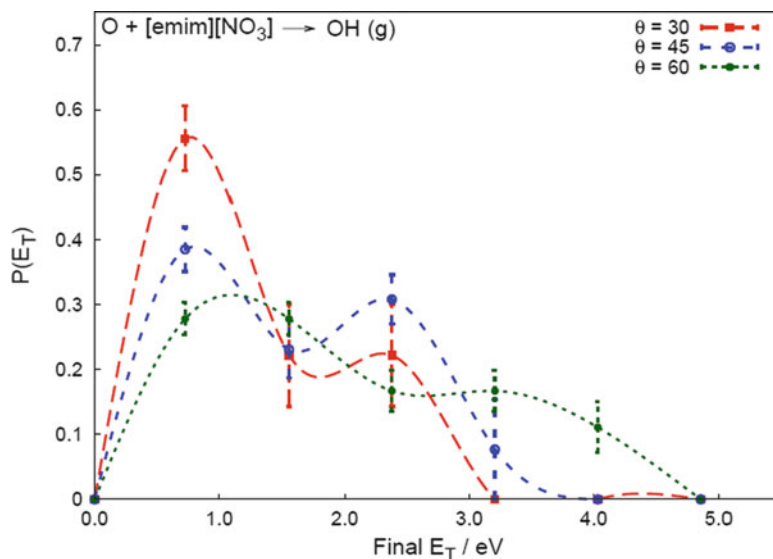


Fig. 9 Distribution of the final translational energy (in eV) of OH for each angle of incidence ($\theta_i = 0^\circ, 30^\circ, 45^\circ$, and 60°)

here, are HNO_2 and HNO_3 , both of which have smaller and much narrower distributions of translational energies and are largely independent of incidence angle. It is thought that this is because the reactive channels that govern these products involve a proton transfer event, and are not dependent directly upon a primary collision event.

5 Summary

In this chapter we reviewed the details of our theoretical methods that are used to describe gaseous atoms scattering from liquid surfaces. Scattering experiments of this type allow for the direct study of the surface reactivity of liquids, including studies of the partitioning of molecular energy transfer into various vibrational, rotational, and translational modes of the scattered products. One of the complexities in modeling such a dynamic system at hyperthermal energies is that many chemical changes can occur (i.e., the making/breaking of several bonds), and a priori knowledge of when and where this will occur is not easy to estimate in the absence of a simulation. Additionally, the spatial length scale needed to describe gas–surface reactions is larger than what can normally be computed purely with *ab initio* QM. Thus we use a hybrid approach that partitions the system into reactive and nonreactive regions to be treated by a dynamics QM/MM approach.

The nonreactive regions (thousands of atoms) were described with predetermined force fields (OPLS-AA) using MM, and the reactive regions (hundreds of

atoms) were computed with semiempirical QM (MSINDO), an efficient approach to describe bond-breaking for the reactions we are interested in. The coordinates and forces in our simulations are propagated in time using a rather robust fifth/sixth order predictor–corrector scheme. One unique aspect of our QM/MM algorithm is that we allow for a dynamic partitioning of atoms to be treated either with MM or QM, which we refer to as the “seed atom” method. Though we took a simplistic approach to the dynamic partition of atoms, we found this to be very useful in studying a surface like squalane that is very porous, allowing the incident atoms lots of freedom to move around within the liquid surface. We further discussed in Sect. 2.3 some of the difficulties involved in reassigning atoms in and out of the reactive region, as this changes the forces computed from one step to the next with a different level of theory.

Thus far, we have applied our QM/MM–MD model to study reactions at the surface of a well known hydrocarbon liquid, squalane, and we have also provided perhaps the first theoretical study of gaseous atom scattering from an RTIL surface. With squalane we observed the reactivity of both $\text{O}(^3\text{P})$ and $\text{F}(^2\text{P})$ scattering from the surface at a few different initial translational energies. The chemistry that ensued upon bombardment with $\text{F}(^2\text{P})$ with 1.0 and 0.5 eV incident energy was limited to H abstraction. However, when $\text{O}(^3\text{P})$ hits the surface of squalane at 5 eV, it is capable not only of H abstraction but also of H elimination and C–C bond scission. Even though understanding the barriers to these reactions helps determine whether there is enough initial translation energy to overcome these barriers, it is only through the dynamics simulations that we gain an insight into the mechanism of these reactions and the likelihood of these reactions occurring as a function of position relative to the liquid interface. One major theme that is noted throughout the discussion in Sect. 4.1 is that the molecular energy (be it vibrational, rotational, or translational) of the nonthermal nascent products emerging from the surface is predominantly due to the bond making/breaking event and is largely independent of the incident atom’s energy and collision angle. This indicates that nonthermal products are incompletely relaxed as they emerge from the liquid surface, even when they are produced a few angstroms beneath the surface.

Probing the reactivity of our RTIL surface of [emim][NO_3] was done with both Ar and $\text{O}(^3\text{P})$ at 5 eV to study both the nonreactive and reactive scattering. The Ar scattering shows that proton transfers can occur between the cations and anions, and there exists a small probability that the neutral species emim or HNO_3 can subsequently desorb during our simulation time of 7.3 ps. Desorption of neutral emim and HNO_3 can also occur in the $\text{O}(^3\text{P})$ scattering simulations and other neutrals such as HNO_2 and O_2 can also be produced. Bombardment of the RTIL with $\text{O}(^3\text{P})$ can also produce many other chemical species. Consistent with the Minton et al. experimental studies, we find that the abstraction product OH desorbs from the RTIL, resulting in an average translational energy that is about half of the input energy at an angle of incidence of 60° , and even less when the angle of incidence is more direct.

The QM/MM applications that we have considered have focused on hyperthermal chemistry for the most part, and this is a natural direction for this research due

to the short time (few ps) and small spatial regions (100–200 quantum atoms) required for describing the hyperthermal dynamics. Even with this limitation, there are a growing number of applications accessible to this method, as high energy atomic sources provide useful information about the structure and reactivity of liquid surfaces. The same technology can also be used to describe gas–solid reactions, as reviewed elsewhere [27], and in this case it is relevant to a number of important industrial etching processes as well as space materials research. Thermal reactions at gas–liquid interfaces can also be described, but the computational effort can easily get out of hand unless one implements additional components in the calculations (such as umbrella sampling so that the reacting species are initiated in close contact). Ultimately one needs to separate the reactive event for such problems from adsorption and diffusion, and there are serious questions as to whether a dynamic QM/MM approach is going to be the most useful way to describe the dynamics.

Acknowledgments This research was supported by AFSOR Grant FA9550-10-1-0205 and by the CENECI CCI NSF grant CHE-0943639.

References

1. Acevedo O, Jorgensen WL (2010) Advances in quantum and molecular mechanical (QM/MM) simulations for organic and enzymatic reactions. *Acc Chem Res* 43:142–151
2. Shaik S, Cohen S, Wang Y, Chen H, Kumar D, Thiel W (2010) P450 enzymes: their structure, reactivity, and selectivity-modeled by QM/MM calculations. *Chem Rev* 110:949–1017
3. Higashi M, Truhlar DG (2008) Electrostatically embedded multiconfiguration molecular mechanics based on the combined density functional and molecular mechanical method. *J Chem Theory Comput* 4:790–803
4. Kamerlin SCL, Haranczyk M, Warshel A (2009) Progress in ab initio QM/MM free-energy simulations of electrostatic energies in proteins: accelerated QM/MM studies of pK(a), redox reactions and solvation free energies. *J Phys Chem B* 113:1253–1272
5. Senn HM, Thiel W (2009) QM/MM methods for biomolecular systems. *Angew Chem* 48:1198–1229
6. Cui Q, Karplus M (2000) Molecular properties from combined QM/MM methods. 2. Chemical shifts in large molecules. *J Phys Chem B* 104:3721–3743
7. Cui Q, Karplus M (2000) Molecular properties from combined QM/MM methods. I. Analytical second derivative and vibrational calculations. *J Chem Phys* 112:1133–1149
8. Gao JL, Truhlar DG (2002) Quantum mechanical methods for enzyme kinetics. *Annu Rev Phys Chem* 53:467–505
9. König PH, Hoffmann M, Frauenheim T, Cui Q (2005) A critical evaluation of different QM/MM frontier treatments with SCC-DFTB as the QM method. *J Phys Chem B* 109:9082–9095
10. Lin H, Truhlar DG (2005) Redistributed charge and dipole schemes for combined quantum mechanical and molecular mechanical calculations. *J Phys Chem A* 109:3991–4004
11. Riccardi D, Schaefer P, Cui Q (2005) pK(a) calculations in solution and proteins with QM/MM free energy perturbation simulations: a quantitative test of QM/MM protocols. *J Phys Chem B* 109:17715–17733
12. Shurki A, Warshel A (2003) Structure/function correlations of proteins using MM, QM/MM, and related approaches: methods, concepts, pitfalls, and current progress. In: *Adv Protein Chem* 66:249–313

13. Bakowies D, Thiel W (1996) Hybrid models for combined quantum mechanical and molecular mechanical approaches. *J Phys Chem* 100:10580–10594
14. Slavicek P, Martinez TJ (2006) Multicentered valence electron effective potentials: a solution to the link atom problem for ground and excited electronic states. *J Chem Phys* 124:084107
15. Svensson M, Humbel S, Froese RDJ, Matsubara T, Sieber S, Morokuma K (1996) ONIOM: a multilayered integrated MO + MM method for geometry optimizations and single point energy predictions. A test for Diels-Alder reactions and $\text{Pt}(\text{P}(\text{t-Bu})(3))_2 + \text{H}_2$ oxidative addition. *J Phys Chem* 100:19357–19363
16. Vreven T, Morokuma K (2000) On the application of the IMOMO (integrated molecular orbital plus molecular orbital) method. *J Comp Chem* 21:1419–1432
17. Shoemaker JR, Burggraf LW, Gordon MS (1999) SIMOMM: an integrated molecular orbital/molecular mechanics optimization scheme for surfaces. *J Phys Chem A* 103:3245–3251
18. Rode B, Hofer TS, Randold BR, Schwenk CF, Xenides D, Vchirawongkwin V (2006) Ab initio quantum mechanical charge field (qmcf) molecular dynamics: a QM/MM-MD procedure for accurate simulations of ions and complexes. *Theor Chem Acc* 115:77–85
19. Lin H, Truhlar DG (2007) QM/MM: what have we learned, where are we, and where do we go from here? *Theor Chem Acc* 117:185–199
20. Rappe AK, Goddard WA III (1991) Charge equilibration for molecular dynamics simulations. *J Phys Chem* 95:3358–3363
21. Heyden A, Truhlar DG (2007) Adaptive partitioning in combined quantum mechanical and molecular mechanical calculations of potential energy functions for multiscale simulations. *J Phys Chem A* 111:2231–2241
22. Rohrig UF, Frank I, Hutter J, Laio A, VandeVondele J, Rothlisberger U (2003) QM/MM car-parrinello molecular dynamics study of the solvent effects on the ground state and on the first excited singlet state of acetone in water. *ChemPhysChem* 4:1177–1182
23. Kerdcharoen T, Morokuma K (2002) ONIOM-XS: an extension of the ONIOM method for molecular simulation in condensed phase. *Chem Phys Lett* 355:257–263
24. Bolten K, Hase WL, Doubleday C Jr (1999) A QM/MM direct dynamics trajectory investigation of trimethylene decomposition in an argon bath. *J Phys Chem B* 103:3691–3698
25. Stanton CL, Kuo I-FW, Munday CJ, Laino T, Houk KN (2007) QM/MM metadynamics study of the direct decarboxylation mechanism for orotidine-5'-monophosphate decarboxylase using two different QM regions: acceleration too small to explain rate of enzyme catalysis. *J Phys Chem B* 111:12573–12581
26. Kerdcharoen T, Liedl KR, Rode BM (1996) A QM/MM simulation method applied to the solution of Li^+ in liquid ammonia. *Chem Phys* 211:313–323
27. Troya D, Schatz GC (2004) Hyperthermal chemistry in the gas phase and on surfaces: theoretical studies. *Int Rev Phys Chem* 23:341–373
28. Kim D, Schatz GC (2007) Theoretical investigation of hyperthermal reactions at the gas-liquid interface: O (3P) and squalane. *J Phys Chem A* 111:5019–5031
29. Radak B, Yockel S, Kim D, Schatz GC (2008) Modeling reactive scattering of F(2P) at a liquid squalane interface: a hybrid QM/MM molecular dynamics study. *J Phys Chem A* 113:7218–7226
30. Garton DJ, Minton TK, Alagia M, Balucani N, Casavecchia P, Gualberto Volpi G (2000) Comparative dynamics of Cl(2P) and O(3P) interactions with a hydrocarbon surface. *J Chem Phys* 112:5975–5984
31. Zhang J, Garton DJ, Minton TK (2002) Reactive and inelastic scattering dynamics of hyperthermal oxygen atoms on a saturated hydrocarbon surface. *J Chem Phys* 117:6239–6251
32. Zhang J, Upadhyaya HP, Brunsvold AL, Minton TK (2006) Hyperthermal reactions of O and O_2 with a hydrocarbon surface: direct C-C bond breakage by O and H-atom abstraction by O_2 . *J Phys Chem B* 110:12500–12511
33. Perkins BG Jr, Nesbitt DJ (2006) Quantum-state-resolved CO_2 scattering dynamics at the gas-liquid interface: incident collision energy and liquid dependence. *J Phys Chem B* 110:17126–17137

34. Zolot AM, Harper WW, Perkins BG, Dagdigan PJ, Nesbitt DJ (2006) Quantum-state resolved reaction dynamics at the gas-liquid interface: direct absorption detection of HF(v, J) product from F(2P) + squalane. *J Chem Phys* 125:021101/1–021101/4
35. Zolot AM, Dagdigan PJ, Nesbitt DJ (2008) Quantum-state resolved reactive scattering at the gas-liquid interface: F + squalane (C₃₀H₆₂) dynamics via high-resolution infrared absorption of nascent HF(v, J). *J Chem Phys* 129:194705/1–194705/11
36. Wu BH, Zhang JM, Minton TK et al (2010) Scattering dynamics of hyperthermal oxygen atoms on ionic liquid surfaces: emim NTf₂ and C(12)mim NTf₂. *J Phys Chem C* 114: 4015–4027
37. Yockel S, Schatz GC (2010) Modeling O(3P) and Ar scattering from the ionic liquid [emim][NO₃] at 5 eV with hybrid QM/MM molecular dynamics. *J Phys Chem B* 114:14241–14248
38. Krebs T, Nathanson GM (2010) Reactive collisions of sulfur dioxide with molten carbonates. *PNAS* 107:6622–6627
39. Muentner AH, DeZwaan JL, Nathanson GM (2007) Interfacial interactions of DO with salty glycerol solutions of KI, NaI, LiI, and NaBr. *J Phys Chem C* 111:15043–15052
40. Waring C, Bagot PAJ, Slattery JM, Costen ML, McKendrick KG (2010) O(P-3) atoms as a probe of surface ordering in 1-alkyl-3-methylimidazolium-based ionic liquids. *J Phys Chem Lett* 1:429–433
41. Waring C, Bagot PAJ, Slattery JM, Costen ML, McKendrick KG (2010) O(P-3) atoms as a chemical probe of surface ordering in ionic liquids. *J Phys Chem A* 114:4896–4904
42. Jay William Ponder (2010) TINKER – software tools for molecular design. Accessed at <http://dasher.wustl.edu/tinker/>
43. Bredow T, Geudtner G, Jug K (2006) MSINDO (version 3.2)
44. Ahlswede B, Jug K (1999) Consistent modifications of SINDO1: I. approximations and parameters. *J Comp Chem* 20:563–571
45. Ahlswede B, Jug K (1999) Consistent modifications of SINDO1: II. Applications to first and second row elements. *J Comp Chem* 20:572–578
46. Kerdcharoen T, Rodes BM (2000) What is the solvation number of Na + in ammonia? An ab initio QM/MM molecular dynamics study. *J Phys Chem A* 104:7073–7078
47. Jorgensen WL, Maxwell DS, Tirado-Rives J (1996) Development and testing of the OPLS all-atom force field on conformational energetics and properties of organic liquids. *J Am Chem Soc* 118:11225–11236
48. Bowman JM, Kuppermann A (1971) Classical and quantum reaction probabilities and thermal rate constants for the collinear H + H₂ exchange reaction with vibrational excitation. *Chem Phys Lett* 12:1–4
49. Porter RN, Raff LM, Miller WH (1975) Quasiclassical selection of initial coordinates and momenta for a rotating morse oscillator. *J Chem Phys* 63:2214–2218
50. Canongia Lopes JN, Deschamps J, Padua AAH (2004) Modelling ionic liquids using a systematic all-atom force field. *J Phys Chem B* 108:2038–2047
51. Jug K, Chiodo S, Calaminici P, Avramopoulos A, Papadopoulos MG (2003) Electronic and vibrational polarizabilities and hyperpolarizabilities of azoles: a comparative study of the structure – polarization relationship. *J Phys Chem A* 107:4172–4183
52. Raabe G, Wang Y, Fleischhauer J (2000) Calculation of the proton affinities of primary, secondary, and tertiary amines using semiempirical and ab initio methods. *Z Naturforsch A* 55:687–694

Multiscale Molecular Methods in Applied Chemistry

Kirchner, B.; Vrabec, J. (Eds.)

2012, XII, 328 p., Hardcover

ISBN: 978-3-642-24967-9